Supersonic Jet Mixing Enhancement Using Impingement Tones from Obstacles of Various Geometries

Ganesh Raman*
NYMA Inc., Brookpark, Ohio 44142
and
Edward J. Rice†
NASA Lewis Research Center, Cleveland, Ohio 44135

This paper reports the results of an experiment that investigated the effect of impingement tones, generated by obstacles of various geometries, on the spreading of a supersonic jet flow. A rectangular supersonic jet was produced using a convergent-divergent nozzle that was operated near its design point (with shocks minimized). Immersing obstacles in the flow produced an intense impingement tone that then propagated upstream (as feedback) to the jet lip and excited the antisymmetric hydrodynamic mode in the jet, thus setting up a resonant self-sustaining loop. The violent flapping motion of the jet due to excitation of the antisymmetric mode, combined with the unsteady wakes of the obstacles, produced large changes in jet mixing. The experiment controlled the frequency and amplitude of the impingement tone excitation by varying the nozzle-to-obstacle distance and the obstacle immersion. Proper shaping of the obstacles made it possible to reduce the thrust penalty significantly.

Nomenclature

A	= area
a	= speed of sound
b	= streamwise extent of obstacle
D_e	= equivalent circular diameter, $\sqrt{4A_e/\pi}$
f	= frequency
h	= smaller exit dimension of rectangular nozzle
k	= integer
L	= spanwise length of obstacle
l	= larger exit dimension of rectangular nozzle
M	= Mach number
$\dot{m}$	= mass flux
n	= integer, edgetone stage
P	= pressure
$St(h)$	= Strouhal number (fh/U_j)
t	= maximum thickness of obstacle
U	= velocity
U_c	= phase velocity
$U_{obstacle}$	= flow velocity sensed by obstacle
x	= axial coordinate
y	= transverse coordinate
z	= spanwise coordinate
γ	= ratio of specific heats
ρ	= density
τ	= thrust

Subscripts

a	= ambient
e, j	= jet exit conditions
o	= plenum
s	= static
t	= pitot

Superscript

$*$	= nozzle throat conditions

I. Introduction

THERE is a renewed interest in supersonic jet mixing due to the high-speed civil transport (HSCT) program.[1] Several methods have been used to enhance jet mixing. For example, the use of tabs,[2,3] counterflow,[4] and acoustic excitation[5] has induced dramatic changes in the spreading rate of the jet. The idea of using acoustic feedback from natural or induced screech sources with potential applications in the design of jet mixer noise suppressors was described by Rice.[6] Rice and Raman[7,8] also conducted demonstration experiments on induced screech excitation. The induced screech concept is based on a class of tones created by flow impinging on surfaces. In the past, such tones have been referred to in a broad sense as edgetones. Considerable work has been done on edgetone generation[9–12]; however, the only work to use edgetones for jet mixing enhancement was that of Krothapalli et al.[12] The present method does not fall precisely into the category of edgetones; it is a variation known as a ringtone.[13] The ringtone in the traditional sense consists of a ring set concentrically with the axis of a circular jet. The method presented in this paper can be thought of as a two-dimensional counterpart of a ringtone. Two obstacles were placed on either side of a rectangular supersonic jet. The immersion of these obstacles into the flow produced an intense impingement tone that then propagated upstream (as feedback) to the jet lip and excited the antisymmetric hydrodynamic mode in the jet, thus setting up a resonant self-sustaining loop.

It is important to note that it is also possible to produce tones without obstacles, for example, screech tones from choked jets. Such tones have been studied by several researchers.[7,14–18] Note that in such cases the shocks in the flow can be thought of as being the obstacles. Therefore, in this paper the impingement tone is referred to as induced screech.

Our previous work[7,8] used square obstacles (with one edge bevelled) with $L = 76.2$ mm and showed that it was possible to get a large mixing benefit. However, the mixing evoked a thrust penalty of almost 20% of the jet's ideal thrust. The thrust penalty cannot be ignored if the induced screech technique is to be adapted for practical applications. Quite obviously, it is necessary to explore ways to achieve mixing with a much lower thrust penalty, and that is the objective of the present study. In the present work, results from the use of obstacles of various shapes will be discussed. The

effect of obstacle shape on the induced tone amplitude, the mixing enhancement, and the thrust penalty will be evaluated.

II.   Experimental Details

A.   Experimental Apparatus

1.   Jet Facility

A schematic representation of the supersonic jet facility is shown in Fig. 1. The 76-cm-diam plenum tank was supplied by compressed air at pressures up to 875 kPa (125 psig) at 26.7°C. After passing through a filter that removed any dirt or dust, the air entered the plenum axially where a perforated plate and a screen distributed it laterally. Two circumferential splitter rings that contained acoustic treatment (Kevlar) removed upstream valve noise. The flow was further conditioned by two screens before undergoing two area contractions of 3.5 and 135. The nozzle included a circular-to-rectangular transition and a converging-diverging nozzle contour, all integrated into one piece. The area ratio of the convergence, $A_{circular}/A^*$, was 2.38 over a length of 20.25 cm. The divergence area ratio, A_e/A^*, was 1.128 over a length of 2.125 cm. The nozzle exit dimensions were 14.1 × 68.1 mm, yielding an aspect ratio of 4.82. Note that the convergence-divergence occurred only in one direction (y) with straight side walls. The nozzle, probe traversing mechanism, and other reflective surfaces in the near field were covered with acoustically absorbent foam. The acoustically absorbent material used was open cell polyurethane foam. The material was 0.635 cm thick (uncompressed). Two layers of this material were used. This minimized strong reflections from the nozzle and plenum. The acoustically absorbent material very effectively absorbs incident sound at frequencies over 1000 Hz; if several layers are used, it absorbs lower frequencies as well.

2.   Screech-Inducing Obstacles

The present study was conducted for obstacles of various geometries. The following obstacle cross sections and dimensions are described in Table 1: A) no obstacles, B) square bevelled, C) circular, D) elliptical, E) wedge, F) diamond airfoil, and G) lenticular airfoil. All of the obstacles described in Table 1 had a spanwise length L of 38.1 mm, and a thickness t of 3.175 mm. The streamwise extent of the obstacles varied depending on shape. For one shape B, a limited set of experiments was carried out for three different obstacle lengths of 12.7, 38.1, and 76.2 mm. The intermediate-length obstacles (38.1 mm) produced the most mixing. Thus, obstacles of various shapes, all having the same length of 38.1 mm, were evaluated. The obstacles will be referred to either by the alphabetical notation or by their shape or both in the text of this paper.

3.   Instrumentation

Figure 2 shows the nozzle with the obstacles located slightly downstream. A 0.64-cm (B & K) microphone located at the jet exit was used to obtain sound pressure levels and spectra. The microphone was omnidirectional (according to manufacturer specifications) within ±1 dB up to 10 KHz and within ±3 dB up to 20 KHz. The microphone was calibrated using a B & K piston-phone calibrator; calibration was corrected for day-to-day changes in atmospheric pressure. Sound pressure levels reported here are in
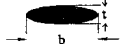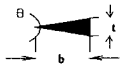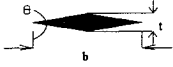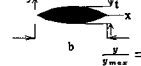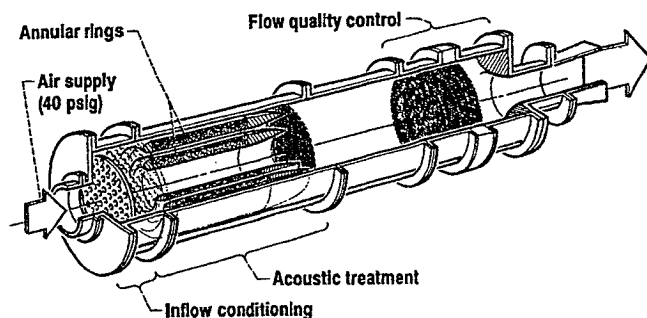

Fig. 1   Schematic of supersonic jet facility.

Table 1   Description of obstacle geometry

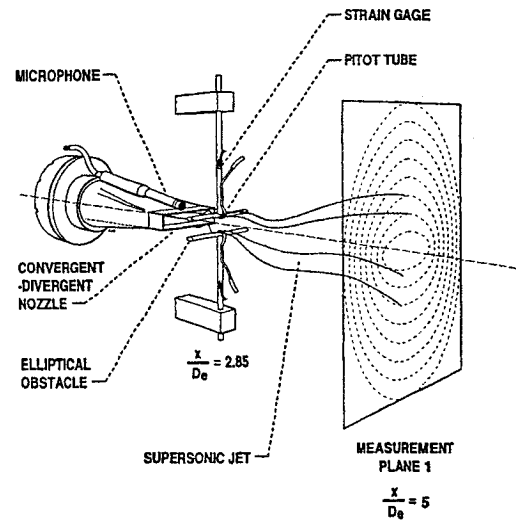| Notation	Crossectional Shape	Sketch with Dimensions (mm)
A	No Obstacle	----------
B	Square Bevelled	t = 3.175 b = 3.175
C	Circular	t = 3.175
D	Elliptical	t = 3.175 b = 12.70
E	Wedge	t = 3.175 b = 9.000 θ = 20°
F	Diamond Airfoil	t = 3.175 b = 18.00 θ = 20°
G	Lenticular Airfoil	t = 3.175 b = 12.70 $\frac{y}{y_{max}} = \frac{x}{40.32}(12.70 - x)$

Fig. 2   Schematic of impingement tone excitation and measurement setup.

decibels relative to 20 μPa (the threshold of human hearing). The obstacles were instrumented with a total pressure tap and a strain gauge to determine the pressure and axial force exerted by the jet flow on the obstacle, respectively. The strain gauges were calibrated by hanging known weights from the obstacle supports with the obstacles clamped in place. The calibration curve was linear for the force range encountered in the present work. A linear curve fit for a typical calibration equation relating the axial force F on the obstacle to the voltage V from the strain gauge was F (kg) = 0.456V (V) + 9.51 × 10^{-4} with a variance of 0.00684 and a maximum deviation of 0.00958. A pitot probe with an o.d. of 0.8 mm was used for the flowfield measurements. The pitot probe was connected to a pressure transducer by a 0.8-mm i.d. tygon tube. Three different pressure transducers, having a maximum range of 350 kPa (50 psig), 105 kPa (15 psig), and 35 kPa (5 psig) were used for the measurements. The centerline pressure at every axial station was used as a guide to select the transducer of an appropriate range for maximum sensitivity.

4. Schlieren System

A focusing schlieren system similar to the one described by Weinstein[19] was used for flow visualization. The schlieren system operated with a strobe in a swept phase mode to produce motion pictures of the flapping mode of the jet. The control system for the schlieren apparatus was modeled after Wlezien and Kibens[20] and was also used successfully in our earlier work.[7,18] The operation of the strobed schlieren system can be summarized as follows. First, the vertical synchronization pulse from the video camera was sensed. Then, a phase delay was started at the first zero crossing of the screech tone, which was measured by a microphone mounted on the nozzle. Finally, after the prescribed phase delay, the strobe was fired. With a fixed phase delay, the motion of the flapping jet could be stopped for viewing. The phase delay could also be continuously swept through one period of screech with the video displaying the flapping motion of the jet instability.

B. Experimental Procedure

The converging-diverging rectangular nozzle was operated at its design Mach number ($\sim$1.392) to minimize natural screech that could interfere with the induced screech. The induced screech was caused by obstacles located on both sides of the longer dimension of the nozzle. The jet was first turned on with the obstacles placed outside the flow. The obstacles were then gradually moved into the flow. At a given axial station the obstacles were immersed to the transverse locations where the normalized velocity measured by the probe on the obstacle, $U_{obstacle}/U_j$, was 0.36 or 0.72. For comparative purposes, the flowfield data for obstacles of various geometries were taken at the same axial location ($x/h = 7.7$) of the obstacles and at the same obstacle immersion ($U_{obstacle}/U_j = 0.72$).

For the various obstacle shapes the induced tone was monitored at the jet exit. Strain gauges mounted on the obstacle supports were used to obtain the axial force experienced by the obstacles. The entire cross section of the jet was surveyed at two downstream locations, x/D_e of 5 and 11. This survey was performed using a total pressure probe. In this paper the induced tone amplitude (measured using a microphone at the jet exit), an estimate of the thrust loss (from the force on the obstacles), and an estimate of the mixing benefit (from the integration of the pressure survey) will be compared.

III. Discussion of Results

The initial part of the discussion will focus on the impingement tone produced by the obstacles. The effect of the impingement tone on the noise spectrum of the supersonic jet will be discussed. Then, the effect of the axial placement and immersion of the obstacle on the frequency and amplitude of the impingement tone will be discussed. Following this discussion flow visualization results for various axial obstacle placements and immersions will be described. Detailed cross sections of the jet showing Mach number contours for the various obstacle shapes will be described at two measurement stations. Finally, the relationship between the impingement tone amplitude, mass-flux enhancement, and thrust penalty will be described, and the significance of these results for potential applications will be discussed.

A. Impingement Tone Characteristics

Figure 3 shows a sound pressure level spectrum obtained using a microphone at the jet exit for two cases, one being the natural jet and the other being the induced tone case. The natural jet was obtained by operating a convergent-divergent nozzle at its design point where shocks are minimized (but not eliminated). The natural jet spectrum shows a relatively weak screech tone with a sound pressure level of 144 dB at $St(h) = 0.15$. When obstacle G is introduced into the flow at an axial location of $x/h = 7.7$, and at an immersion where $U_{obstacle}/U_j = 0.72$, the tone amplitude is intensified (159 dB) at the same Strouhal number (0.15).

It is interesting to note that besides the tones, the characteristics of the two spectra are different. For the natural jet under ideally expanded conditions (shocks minimized), one would expect insignificant shock associated broadband noise. The only significant contributions are from the jet mixing noise and the broadband noise that is associated with the finer scales of turbulence. In contrast,
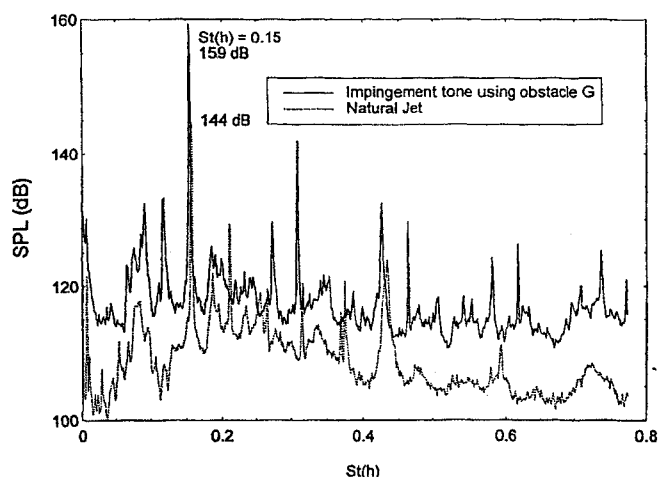

Fig. 3 Sound pressure level spectrum measured at jet exit; $M_j = 1.392$, $x/h = 0, y/h = 1, z/h = 0$, levels in decibels re. 20 μPa.

when the obstacles are immersed there are noise contributions from all of the mechanisms. Thus, the broadband noise levels are higher when the obstacles are immersed.

The fact that the induced tone observed in Fig. 3 excites the jet in an antisymmetric mode was verified by a pair of microphones located on either side of the narrow dimension of the nozzle. The phase difference between the two microphones (obtained from the cross-spectrum phase) was about 180 deg ($\pm$5 deg measurement and positioning accuracy).

In Fig. 4 the Strouhal number (fh/U_j) of the screech tone induced at the jet lip, is plotted vs a dimensionless nozzle-to-obstacle distance. Although the data are for obstacle B ($L = 76.2$ mm), they reproduce quite well for the other shapes. The numbers above the experimental data represent the tone amplitudes (decibels relative to 20 μPa) measured at the jet lip. The difference between Figs. 4a and 4b lies in the immersion of the obstacles. The obstacle immersion was such that both obstacles sensed a normalized flow velocity, $U_{obstacle}/U_j$ of 0.36 (Fig. 4a) or 0.72 (Fig. 4b). For both cases there were simultaneous multiple frequencies that were not harmonically related. Values of expected edgetone frequencies based on Powell's[9] theory were calculated using

$$n/f = x/U_c + x/a \tag{1}$$

where f represents the frequency of the tone and n denotes the stage. The nozzle to edge distance x and the phase velocity of the coherent disturbances U_c along with the speed of sound a determines the frequency of the edgetone. Note that in a very low-speed flow $a \gg U_c$ and $n/f = x/U_c$ is sufficient to calculate the frequency. This is not so in a high-speed jet. The calculated stage Strouhal numbers (fh/U_j) based on Eq. (1) are shown as dashed lines in Figs. 4a and 4b for several stages. A phase velocity U_c/U_j of 0.55 produced the best agreement for Fig. 4a, whereas an assumed phase velocity U_c/U_j, of 0.44 produced the best agreement for 4b. Both immersions produced tones in the Strouhal number range (0.15–0.2) most effective for enhancing jet mixing. The tone amplitudes are very high for $n = 3$. A plausible explanation is that in addition to the requirements of Eq. (1), a standing wave could be formed between the obstacle and the nozzle lip. The frequency of such a standing wave is

$$f = ak/2x \tag{2}$$

A double resonance will occur when Eqs. (1) and (2) are satisfied simultaneously. For the present set of data it appears that such a resonance occurs for $n = k = 3$. A similar observation was also made by Fox et al.[21] for the case of a jet impinging on a flat plate. In addition, the sound pressure levels produced by greater immersion of the obstacles were higher and were expected to cause higher mixing. Note that the greater immersions would also represent higher values of thrust loss. It is this mixing benefit vs thrust penalty that will be the focus of later sections. Although the mechanisms for natural
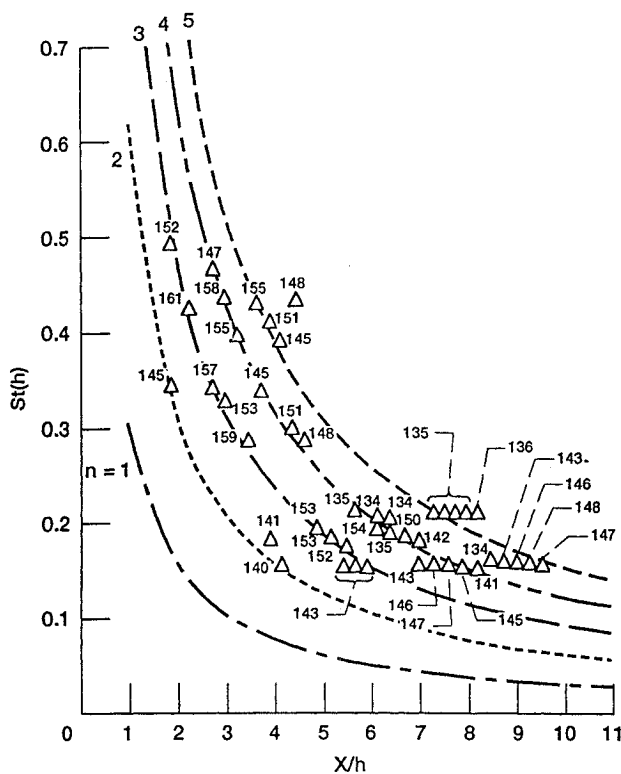
a)
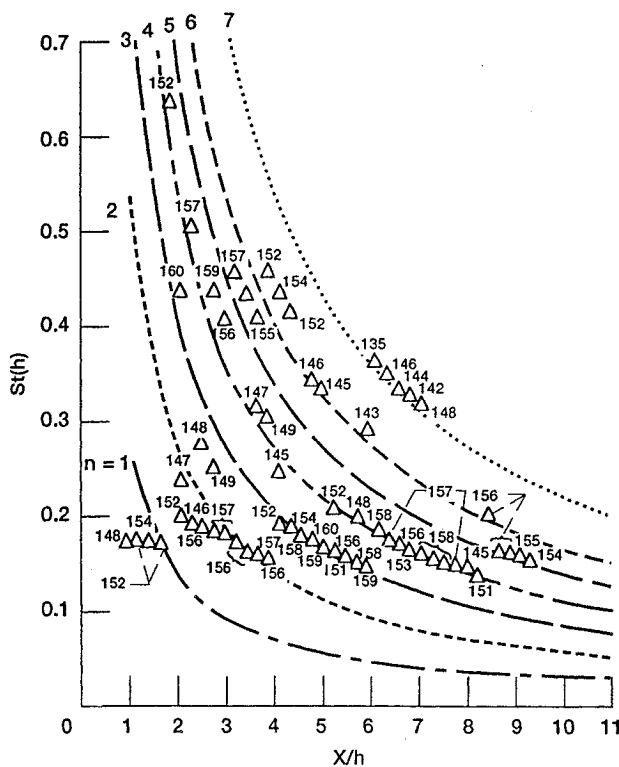
b)

Fig. 4 Effect of axial location of obstacle on the Strouhal number of the induced tone; $M_j = 1.392$, **obstacle immersions, ▲ data for obstacle B (see Table 1), dashed lines are the edgetone stages described by Eq. (1), numbers represent the tone amplitude (dB re. 20** μ**Pa) measured at** $x/h = 0, y/h = 1, z/h = 0$: $U_{obstacle}/U_j$, **of a) 0.36 and b) 0.72.**

and induced screech are fairly well understood and the frequency correlates reasonably well with the shock spacing (natural screech) or the nozzle-to-obstacle spacing (induced screech), it is difficult to define the parameters that control the amplitude.

The impingement tone characteristics for obstacles of various shapes at an obstacle location of $x/h = 7.7$ and an immersion at which the obstacles sensed a normalized velocity,

Table 2 Impingement tone characteristics for various obstacles, location $x/h = 7.7, x/D_e = 2.85$, **immersion,** $U_{obstacle}/U_j = 0.72$

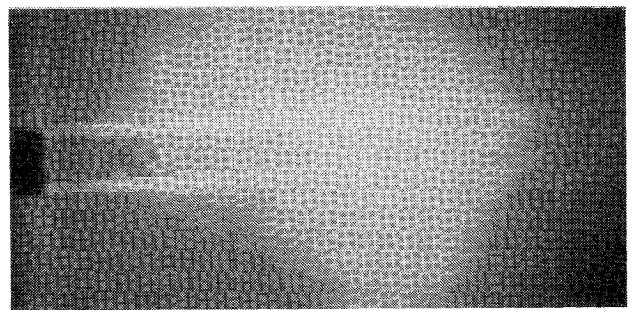| Obstacle (Notation and Geometry)	f (Hz)	St(h)	SPL (dB) (measured at jet lip)
A No Obstacle	5280	0.150	144.0
B	5248	0.149	157.0
C	5100	0.145	156.0
D	5152	0.146	151.6
E	5216	0.148	154.2
F	5248	0.149	156.8
G	5280	0.150	159.0

Fig. 5   Schlieren photograph of the natural unexcited jet, $M_j = 1.392$, **range covered:** $x/h = 0-10$.

$U_{obstacle}/U_j = 0.72$, are given in Table 2. At this axial location ($x/h = 7.7$) the induced tone frequency matched the natural flow instability and consequently had the maximum effect on the spreading of the jet. The effect on the jet spread is discussed in Sec. III.C. It is important to emphasize that despite the similarities between the phenomenon under study and the edgetone, they still differ. For example, in the present case one side of the obstacle senses a higher velocity than the other and there could be a nozzle effect when two aerodynamically shaped obstacles are used on both sides of the jet, causing local acceleration (or deceleration) of the flow.

B.   Flow Visualization

Figure 5 is a strobed schlieren photograph of the natural jet. The convergent-divergent nozzle is operated at design conditions (with shocks minimized). The ideally expanded jet is seen in the photograph. Note that since it is not possible to eliminate shocks in a rectangular jet, residual screech causes some flapping motions in the jet. Figure 6 shows schlieren photographs of the jet with obstacles (shape B, $L = 76.2$ mm) at $x/h = 2.9$ for two different obstacle immersions ($U_{obstacle}/U_j = 0.36$ and 0.72). From the picture, small wavelength (high-frequency) oscillations are visible in such a jet. Figures 7 and 8 show the same type of photographs as Fig. 6, but for obstacles at other x/h locations ($x/h = 5$ and 7.7, respectively). From Figs. 6–8 it can be observed that a larger nozzle-to-obstacle (x/h) distance excites waves of a larger wavelength (lower frequency). In addition, the amplitude of the oscillations
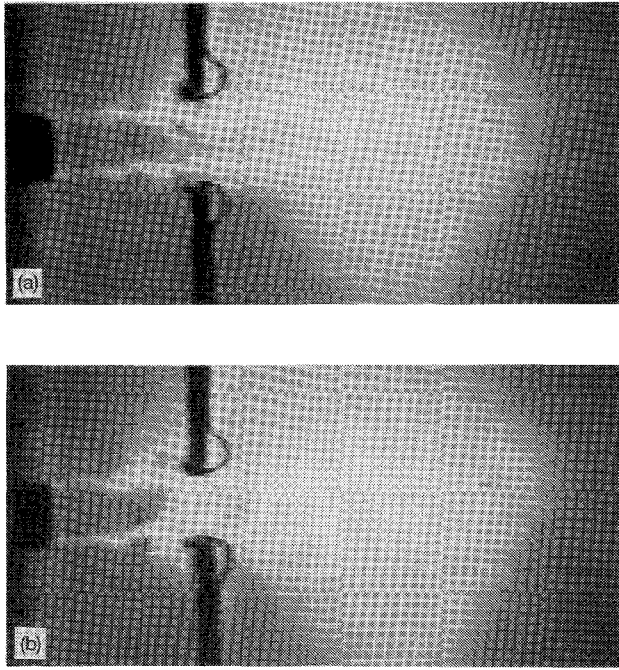
Fig. 6 Strobed schlieren photographs of jet excited by impingement tone, M_j = 1.392, obstacle B (see Table 1), obstacle at x/h = 2.9, obstacle immersions, $U_{obstacle}/U_j$ of a) 0.36 and b) 0.72.
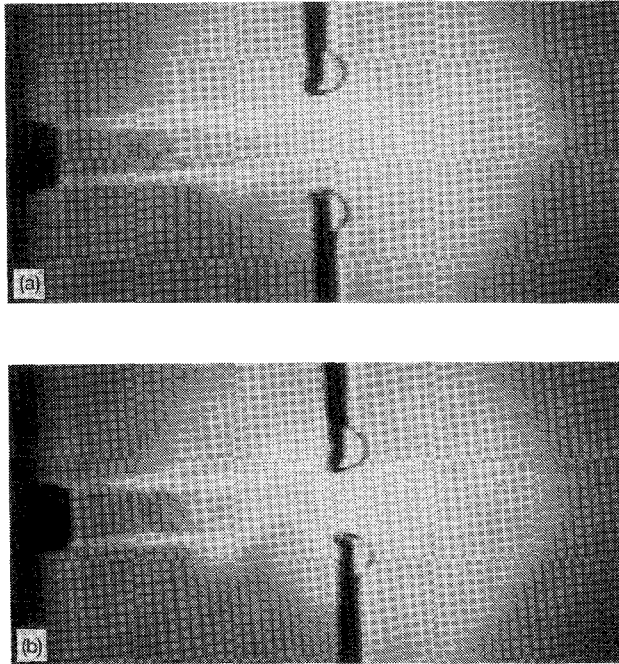

Fig. 7 Strobed schlieren photographs of jet excited by impingement tone, M_j = 1.392, obstacle B (see Table 1), obstacle at x/h = 5.0, obstacle immersions, $U_{obstacle}/U_j$ of a) 0.36 and b) 0.72.

increases as the immersion is changed from $U_{obstacle}/U_j$ = 0.36 to 0.72. These photographs prove visually that it is possible to excite the jet at various frequencies and amplitudes of the antisymmetric mode by varying the axial location and the immersion of the obstacles (i.e., the trends shown in Fig. 4a and 4b are confirmed visually).

C. Description of the Mean Flowfield

Figures 9 and 10 show the Mach number contours measured at x/D_e = 5 and 11, respectively, for the various cases. The inner
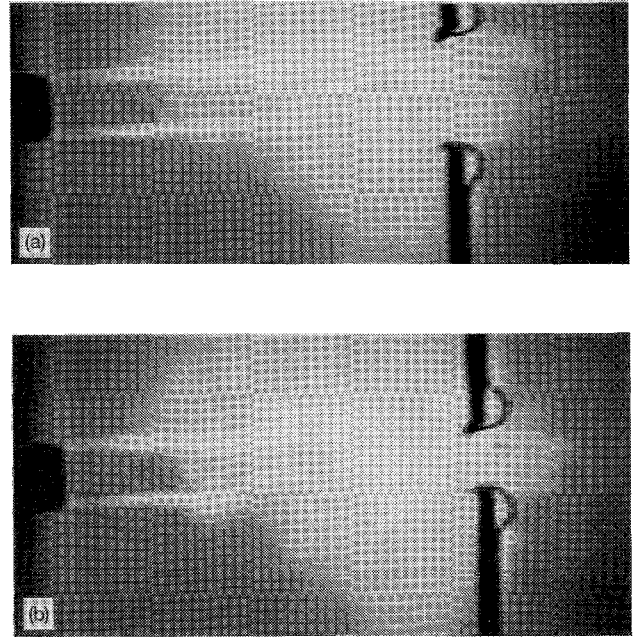

Fig. 8 Strobed schlieren photographs of jet excited by impingement tone, M_j = 1.392, obstacle B (see Table 1), obstacle at x/h = 7.7, obstacle immersions, $U_{obstacle}/U_j$ of a) 0.36 and b) 0.72.

and outermost contours are specified. In addition the cross-sectional shape of the obstacle is indicated in the figure. The notation and obstacle geometries are described in Table 1. In all cases the obstacle length L was 38.1 mm. For each case the obstacles were located at x/h = 7.7 (x/D_e = 2.85) at an immersion where they experienced a normalized flow velocity of $U_{obstacle}/U_j$ = 0.72. Mach numbers were obtained from the measured pitot pressures using

$$M = \sqrt{\frac{2}{(\gamma - 1)}\left(\left[\frac{P_a}{P_t + P_a}\right]^{\gamma-1/\gamma} - 1\right)} \quad (3)$$

Note that it was assumed that γ = 1.4 and that the local static pressures could be approximated by the ambient room pressure. Such an approximation is fairly accurate at x/D_e = 11 (Fig. 10) but not so for the data at x/D_e = 5 (Fig. 9). However, the data are still good for comparative purposes. The obstacles produce a significant increase in jet spreading. Note the change in scales between Figs. 9 and 10. Also note that for obstacles B and C the supporting rods (see Fig. 2) were cylindrical (3.175 mm diam), whereas for obstacles D–G, the supports were airfoil-shaped struts. Thus, not only is the drag low due to these struts but the spreading of the jet along the supporting rods is minimized. Hence, a marked change occurs between the cross-sectional distortion for obstacles B and C vs that for D–G.

D. Tone Amplitude, Thrust Loss, and Mixing Enhancement

The induced tone amplitude with the various obstacles in place was measured using a microphone located at the jet exit. The thrust loss estimate was obtained in the following manner: First, the ideal thrust of the jet issuing from a convergent-divergent nozzle operating at its design point was calculated using

$$\tau = A^* P_o \sqrt{\frac{2\gamma^2}{\gamma - 1}\left(\frac{2}{\gamma + 1}\right)^{(\gamma+1)/(\gamma-1)}\left[1 - \left(\frac{P_e}{P_0}\right)^{(\gamma-1)/\gamma}\right]} \quad (4)$$

Then, the axial force that the jet exerted on the obstacles was obtained by a direct measurement using strain gauges mounted on the obstacle supports. Finally, the ratio obtained by dividing the force that the obstacles sense by the jet's ideal thrust (expressed as a percentage) provided our thrust loss number. The jet's ideal thrust was 26.45 Kg, and the force on the obstacles varied depending on the shape and immersion of the obstacles.
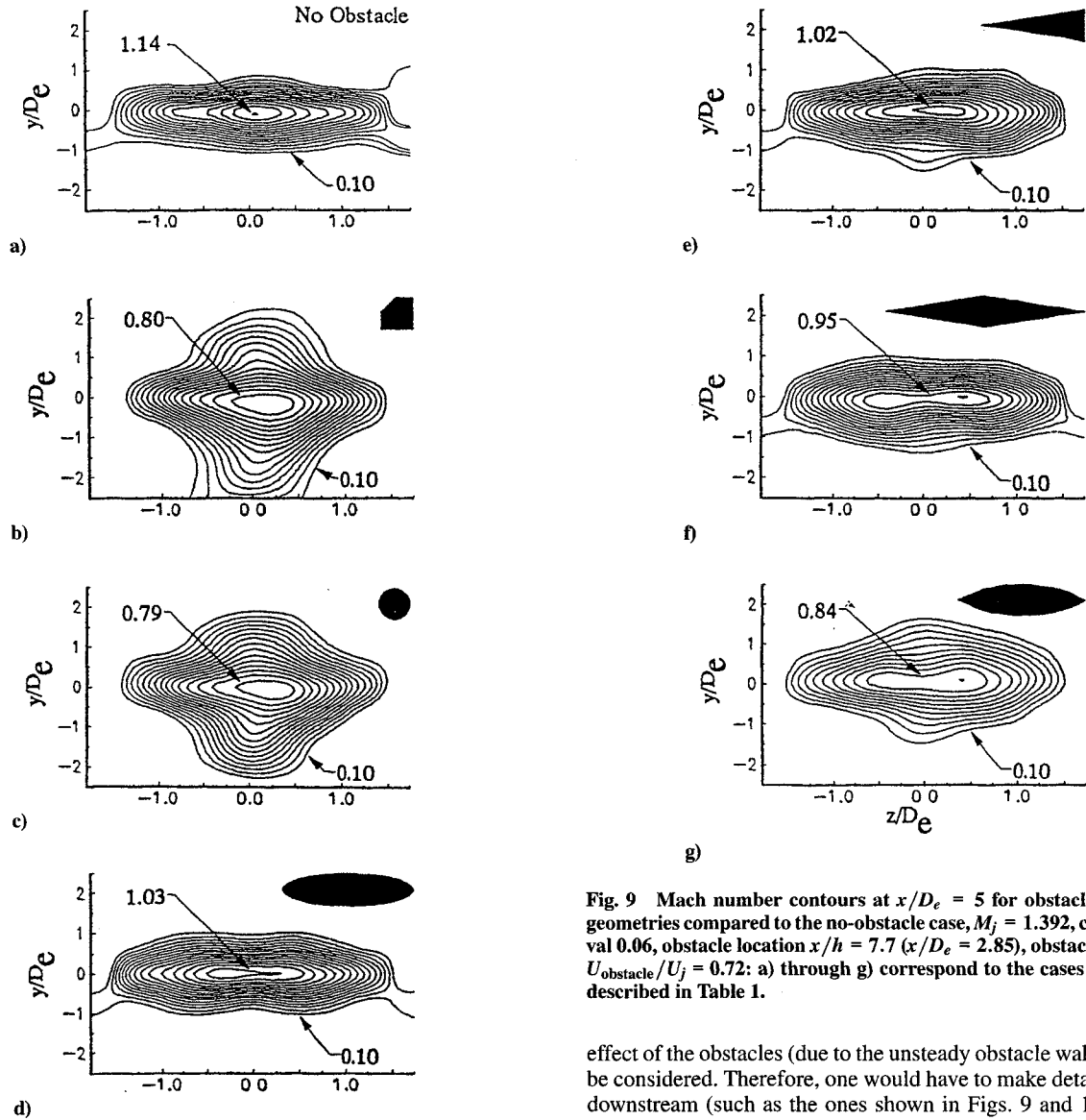
Fig. 9 Mach number contours at x/D_e = 5 for obstacles of various geometries compared to the no-obstacle case, M_j = 1.392, contour interval 0.06, obstacle location x/h = 7.7 (x/D_e = 2.85), obstacle immersion $U_{obstacle}/U_j$ = 0.72: a) through g) correspond to the cases and symbols described in Table 1.

The mass-flux ratio that is used here as an indicator of jet mixing enhancement was obtained using the pitot tube data and was calculated as follows:

$$\frac{\dot{m}}{\dot{m}_e} = \int \int \frac{(\rho U)\, dy\, dz}{\rho_e U_e A_e} \tag{5}$$

where

$$\frac{\rho U}{\rho_e U_e} = \frac{P_s}{P_e} \frac{M}{M_e} \left(\frac{1 + 0.2 M^2}{1 + 0.2 M_e^2} \right)^{0.5} \tag{6}$$

Note that M is obtained from Eq. (3) and $\gamma = 1.4$. It was assumed that the local static pressure P_s could be approximated by the ambient static pressure P_a.

Figure 11a shows a plot of the thrust loss for a pair of obstacles vs the amplitude of the induced tone measured at the jet lip. The obstacles were located at x/h = 7.7 (x/De = 2.85) at an immersion where the obstacles experienced a flow velocity of $U_{obstacle}/U_j$ = 0.72. Appropriate shaping induces a very high-amplitude tone at the jet lip with little thrust loss. For example, the square obstacle B induces a screech tone of 157 dB at the jet lip with an associated thrust loss of 14.4%. In contrast an aerodynamically shaped obstacle G can induce a tone of 159 dB with a 3.2% thrust penalty. However, the screech level at the lip alone is not a sufficient indicator of the jet's spreading rate. First, because of the saturation effect, beyond a certain level of screech amplitude, there may be no further effect on the spreading of the jet. Second, the hydrodynamic

effect of the obstacles (due to the unsteady obstacle wakes) needs to be considered. Therefore, one would have to make detailed surveys downstream (such as the ones shown in Figs. 9 and 10) to assess the combined effect of screech and the hydrodynamic effect of the obstacles.

Figure 11b shows a plot of the mass-flux ratio vs the amplitude of the screech tone induced at the jet lip. The axial location and immersion of the obstacles were the same as that described in connection with Fig. 11a. Mass-flux data are shown at x/D_e = 5 (filled symbols) and x/D_e = 11 (open symbols). The obstacle inducing the highest tone amplitude G does not produce the maximum increase in the mass-flux ratio, but the square B and circular C cross-sectional obstacles with cylindrical supports provide the highest mass-flux values. Thus, it is to be recognized that the effect on the mass-flux ratio is not due to the screech tone alone but due to a combination of the screech tone and the unsteady wake of the obstacles and the obstacle supports. It is difficult to separate the tone effect from the wake effect. This difficulty arises because the process involves a resonant self-sustaining loop in which the flow interacts with the obstacles to produce the tone, which in turn propagates upstream and modifies the flow. However, it is clear that obstacle bluntness (B and C) has a greater effect than screech amplitude. Unfortunately, the same bluntness is also responsible for a higher thrust penalty.

Figure 11c shows the thrust loss vs mass-flux ratio for various obstacles. The mass-flux ratio measured at x/D_e = 5 (filled symbols) and x/D_e = 11 (open symbols) is plotted on the abscissa. The mass-flux ratio for the no-obstacle case was 1.64 at x/D_e = 5 and 2.4 at x/D_e = 11. For the obstacle cases, the thrust loss value given is for a pair of obstacles. The obstacles that produce high mixing have a high-thrust loss. The shaped obstacles have a substantially lower thrust penalty but also produce lower mixing. A limited set of experiments was conducted in which the resonance was first induced

using a pair of obstacles B following which one of the obstacles was withdrawn. The removal of one obstacle reduced the thrust penalty by 50% (as expected) but reduced the mixing benefit by only 20%.

E. Mixing Benefit vs Thrust Penalty

To derive a quantitative comparison between the obstacles one must define a mixing benefit parameter that is adjusted for thrust loss. A mixing benefit parameter at any downstream station can be defined as

mixing benefit parameter

$$= \frac{(\dot{m}/\dot{m}_0)_{\text{with obstacle}} - (\dot{m}/\dot{m}_0)_{\text{without obstacle}}}{(\dot{m}/\dot{m}_0)_{\text{without obstacle}}} \qquad (7)$$

The difference between the mass-flux ratios of the cases with and without the obstacles is really a measure of the mixing benefit. This is normalized by the mass-flux ratio for the no-obstacle case and is expressed as a percentage. Therefore, introducing the obstacle increases the mass-flux ratio at a given downstream station by a certain percentage of the no-obstacle case. This will be referred to as the mixing benefit parameter. When this parameter is normalized by the percent thrust loss, it provides a thrust loss adjusted mixing benefit parameter. This parameter, tabulated in Table 3, offers an

Table 3 Comparison of mixing benefit vs thrust loss

Obstacle		Thrust Loss (% of jet thrust)	Mixing Benefit Parameter $(x/D_e = 5)$	Mixing Benefit per % Thrust Loss $(x/D_e = 5)$
A	No Obstacle	--	--	--
B		14.400	31.09	2.15
C		12.000	21.34	1.78
D		1.450	6.64	4.57
E		1.720	13.23	7.69
F		0.965	8.20	8.50
G		3.200	17.13	5.35

Mixing Benefit Parameter = $\dfrac{(\dot{m}/\dot{m}_o)_{\text{With Obstacle}} - (\dot{m}/\dot{m}_o)_{\text{Without Obstacle}}}{(\dot{m}/\dot{m}_o)_{\text{Without Obstacle}}} \times 100$
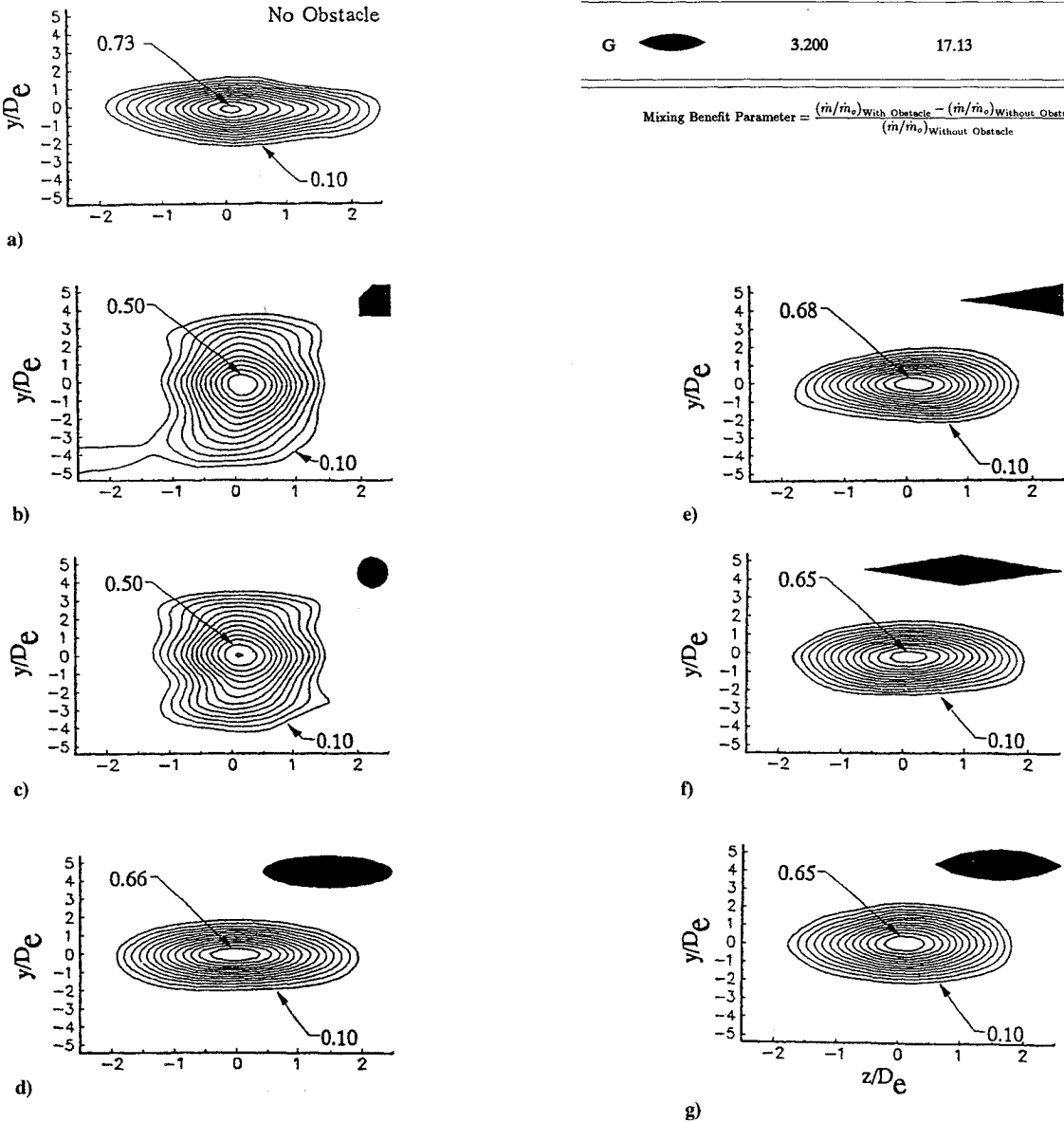

Fig. 10 Mach number contours at x/D_e = 11 for obstacles of various geometries compared to the no-obstacle case, M_j = 1.392, contour interval 0.04, obstacle location x/h = 7.7 $(x/D_e$ = 2. 85), obstacle immersion U_{obstacle}/U_j = 0.72: a) through g) correspond to the cases and symbols described in Table 1.
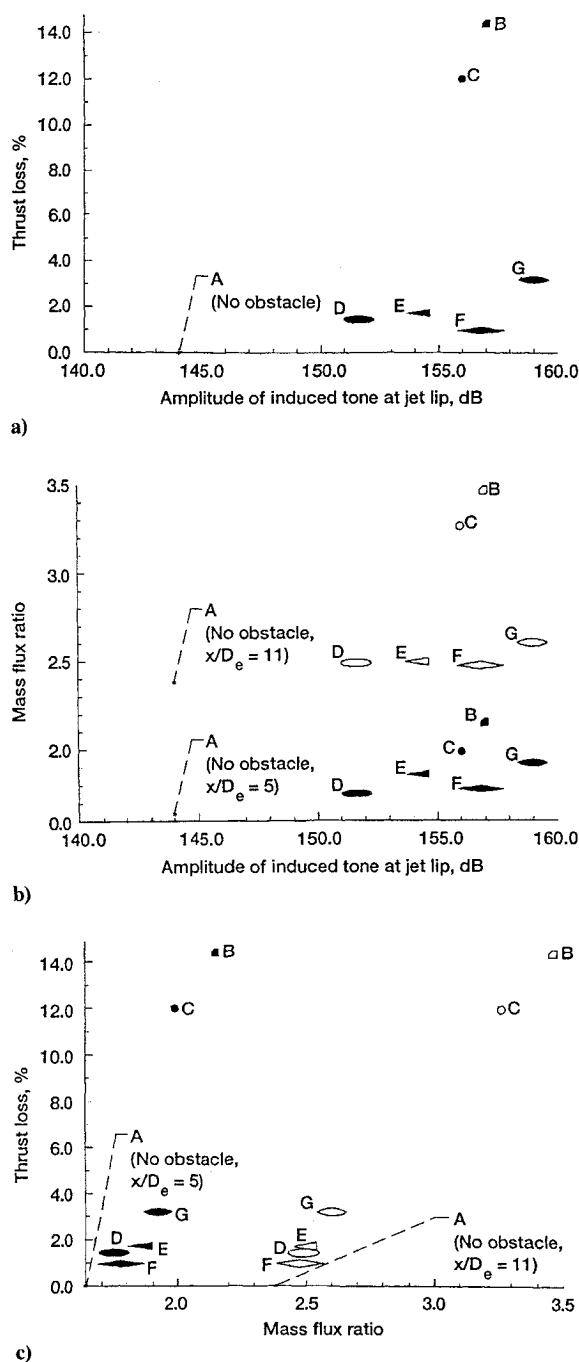
a)

b)

c)

Fig. 11 Comparison of mass-flux, thrust loss, and impingement tone level for obstacles of various geometries, $M_j = 1.392$, obstacle location $x/h = 7.7$, obstacle immersion $U_{obstacle}/U_j = 0.72$: a) thrust loss vs amplitude of induced tone, b) mass-flux ratio vs amplitude of induced tone, and c) thrust loss vs mass-flux ratio.

obstacle efficiency number. Higher values indicate more efficient obstacles. However, obstacles should not be selected based on this number alone. For example, obstacle B, which has a thrust loss adjusted mixing benefit of 2.15, has a mixing benefit parameter of 31.09 with a very high-thrust penalty of 14.4%. In contrast, obstacle F, which has a thrust loss adjusted mixing benefit of 8.5, has a very low-thrust penalty (0.965%), but the mixing benefit parameter (8.2) is not attractive for practical applications. Obstacle G, the lenticular airfoil, appears attractive with a mixing benefit parameter of 17.03 and a thrust penalty of 3.2%, yielding a thrust loss adjusted mixing benefit of 5.35. Although obstacles D and G have the same thickness and chord, their performances differ considerably. Obstacle G evokes a higher thrust loss and produces higher mixing enhancement at $x/D_e = 5$ than obstacle D. The mixing enhancement at the

station closer to the nozzle exit ($x/D_e = 5$) is more important than that at $x/D_e = 11$ in mixer ejector nozzle applications.

F. Applicability—Noise Reduction in Mixer Ejectors

In practical applications the obstacles can be used when required and retracted at other times. For example, to rapidly mix the exhaust of a military aircraft to reduce its thermal signature, the obstacles need to be immersed only at critical times during combat. In applications relating to HSCT the technique could be used to satisfy the sideline noise requirements for takeoff and approach and withdrawn at other times.

It should be emphasized that this technique is proposed for use internally in an acoustically lined mixer-ejector nozzle system. In such a situation the noise benefit would appear as a consequence of the mixing. The dramatic increase in mixing moves the jet noise source location back toward the mixer nozzle lip (within the ejector). This provides a longer acoustic path for the internal jet mixing noise as it propagates downstream through the acoustically treated duct section. Properly designed acoustic treatment could take advantage of this upstream source shift since the final goal will be to ensure that the system as a whole is not as noisy as a system without induced screech.

The applicability of this technique will depend on the assessment of several important effects not considered here such as flow temperature, scalability, and two-stream jet effects. Future work should focus on addressing these effects.

IV. Concluding Remarks

The concept of using impingement tones to enhance the mixing of a supersonic rectangular jet was explored further. Obstacles of various cross-sectional shapes were placed in the flow. The obstacles were placed at an axial station where the induced tone matched the natural flow instability. In addition, the obstacle immersion that produced the highest levels of excitation was used. The impingement tone excited the jet in the antisymmetric mode. The combination of this excitation and the effect of the wake of the obstacles caused significant changes in the jet cross section and spreading rate. The main focus of this work was on evaluating mixing benefit and its relationship to the thrust penalty. A comparison between the various obstacle shapes was made using a mixing benefit parameter and a thrust loss adjusted mixing benefit parameter. The lenticular airfoil (convex lens shaped) with diamond airfoil shaped supports provided the best results for the range of parameters tested in this study.

Acknowledgments

References

[1]Seiner, J. M., and Krejsa, E. A., "Supersonic Jet Noise and the High Speed Civil Transport," AIAA Paper 89-2358, 1989.

[2]Ahuja, K. K., and Brown, W. H., "Shear Flow Control by Mechanical Tabs," AIAA Paper 89-0994, 1989.

[3]Samimy, M., Zaman, K. B. M. Q., and Reeder, M. F., "Effect of Tabs at the Nozzle Lip on the Flow and Noise Field of an Axisymmetric Jet," AIAA Journal, Vol. 31, No. 4, 1993, pp. 609–619.

[4]Strykowski, P. J., Krothapalli, A., and Wishart, D., "The Enhancement of Mixing in High Speed Heated Jets Using a Counterflowing Nozzle," AIAA Paper 92-3262, 1992.

[5]Lepicovsky, J., Ahuja, K. K., Brown, W. H., and Burrin, R. H., "Coherent Large-Scale Structures in High Reynolds Number Supersonic Jets," AIAA Journal, Vol. 25, 1987, pp. 1419–1425.

[6]Rice, E. J., "Jet Mixer Noise Suppressor Using Acoustic Feedback," NASA Lewis Research Center, Patents pending, Application No. 08/046, 256 filed/April 14, 1993 and 08/194, 654 filed Feb. 10, 1994.

[7]Rice, E. J., and Raman, G., "Enhanced Mixing of a Rectangular Supersonic Jet by Natural and Induced Screech," AIAA Paper 93-3263, 1993.

[8]Rice, E. J., and Raman, G., "Mixing Noise Reduction for Rectangular Supersonic Jets by Nozzle Shaping and Induced Screech Mixing," AIAA Paper 93-4322, 1993.

[9]Powell, A., "On the Edgetone," *Journal of the Acoustical Society of America*, Vol. 33, No. 4, 1961, pp. 395–409.

[10]Rockwell, D., "Oscillations of Impinging Shear Layers," *AIAA Journal*, Vol. 21, No. 5, 1983, pp. 645–664.

[11]Crighton, D. G., "The Jet Edge-Tone Feedback Cycle; Linear Theory for the Operating Stages," *Journal of Fluid Mechanics*, Vol. 234, Jan. 1992, pp. 361–391.

[12]Krothapalli, A., Karamcheti, K., Hsia, Y., and Baganoff, D., "Edge Tones in High Speed Flows and their Application to Multiple-Jet Mixing," *AIAA Journal*, Vol. 21, No. 7, 1983, pp. 937, 938.

[13]Blake, W. K., "Mechanics of Flow-Induced Sound and Vibration, Vol. I: General Concepts and Elementary Sources," *Applied Mathematics and Mechanics*, Vol. 17-I, Academic, New York, 1986.

[14]Powell, A., "On the Noise Emanating from a Two-Dimensional Jet above the Critical Pressure," *Aeronautical Quarterly*, Vol. 4, Feb. 1953, pp. 103–122.

[15]Glass, D. R., "Effects of Acoustic Feedback on the Spread and Decay of Supersonic Jets," *AIAA Journal*, Vol. 6, No. 10, 1968, pp. 1890–1897.

[16]Tam, C. K. W., "The Shock-Cell Structures and Screech Tone Frequencies of Rectangular and Non-Axisymmetric Supersonic Jets," *Journal of Sound and Vibration*, Vol. 121, No. 1, 1988, pp. 135–147.

[17]Krothapalli, A., Hsia, Y., Baganoff, D., and Karamcheti, K., "The Role of Screech Tones in Mixing of an Underexpanded Rectangular Jet," *Journal of Sound and Vibration*, Vol. 106, No. 1, 1986, pp. 119–143.

[18]Raman, G., and Rice, E. J., "Instability Modes Excited by Natural Screech Tones in a Supersonic Rectangular Jet," *Physics of Fluids*, Vol. 6, No. 12, 1994, pp. 3999–4008.

[19]Weinstein, L. M., "An Improved Large-Field Focusing Schlieren System," AIAA Paper 91-0567, 1991.

[20]Wlezien, R. W., and Kibens, V., "Influence of Nozzle Asymmetry on Supersonic Jets," *AIAA Journal*, Vol. 26, No. 1, 1988, pp. 27–33.

[21]Fox, M. D., Kuroska, M., Hedges, L., and Hirano, K., "The Influence of Vortical Structures on the Thermal Fields of Jets," *Journal of Fluid Mech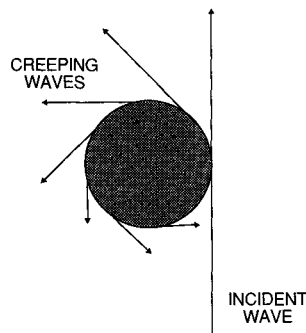anics*, Vol. 255, 1993, pp. 447–472.